Polystyrene/Poly(*n*-butyl acrylate) Latex Blend Coalescence, Particle Size Effect, and Surfactant Stratification: A Spectroscopic Study

Yaqiu Zhao and Marek W. Urban*

Shelby F. Thames Polymer Research Center, School of Polymer and High Performance Materials, University of Southern Mississippi, Hattiesburg, Mississippi 39406

Received January 24, 2000; Revised Manuscript Received June 6, 2000

ABSTRACT: These studies show that polystyrene/poly(*n*-butyl acrylate) (p-Sty/p-nBA) latex blend coalescence is inherently affected by latex composition, p-Sty particle size, and the temperature difference between coalescence (T_c) and glass transition (T_g) temperatures. Sodium dioctylsulfosuccinate (SDOSS) surfactant molecules are expelled to the film−air (F−A) interface when $T_c > T_g$ of the p-Sty phase. Quantitative attenuated total reflectance Fourier transform infrared (ATR FT-IR) analysis shows that SDOSS−H_2O concentration levels near the F−A interface diminish for larger p-Sty latex particle sizes and the magnitude of the SDOSS−COOH interactions near the F−A interface exhibits similar trends. Furthermore, the amount of SDOSS expelled to the F−A interface is directly proportional to the p-Sty phase surface area. These studies also show that SDOSS hydrophilic ends are preferentially parallel to the F−A interface, while hydrophobic ends are preferentially perpendicular.

Introduction

In recent studies[1] we addressed the issue of coalescence and surfactant stratification in Sty/n-BA copolymer latex films. However, latex polymer blends are particularly interesting because a combination of soft and hard particles provides a number of useful properties, and understanding of the processes governing their coalescence, subsequent film formation,[2] and film morphology not only are of interest from a scientific point of view but also have numerous practical implications. A series of the previous studies on latex films indicated that the mobility of low molecular weight species, in particular surfactant molecules, may be affected by latex glass transition temperature (T_g), which is inherently related to the free volume of a polymer matrix,[3,4] surface tension at the film−air (F−A) and film−substrate (F−S) interfaces,[5−10] compatibility of individual components,[11−18] and coalescence times.[18−20] It turns out that there are other factors that influence the distribution of individual components across the latex film, and interactions among them become increasingly important during the film formation. Although, for typical copolymer latexes with T_g below the minimum film-formation temperature (MFT), continuous-phase morphology is believed to be affected by the particle packing and subsequent particle deformation followed by interparticle diffusion and film formation. For latex blends containing soft and hard particles, these processes may be more complex because hard particles with T_g above the MFT will remain rigid, thus limiting interparticle diffusion during latex coalescence. This process becomes even further complicated when surfactant molecules leave latex particles and migrate to the F−A and F−S interfaces during coalescence. Thus, for latex blends, one would anticipate at least a four-component system, in which water, surfactant, and soft/hard latex particles are the key components, and their distribution may vary at various stages of the film formation and depths from the surface.

* To whom all correspondence should be addressed.

Table 1. Starting Materials and Characteristics of p-nBA and p-Sty Latex Particles

	latexes			
	p-nBA	p-Sty	p-Sty	p-Sty
particle size (nm)	150	102	77	61
particle size distribution (D_w/D_n)	1.005	1.19	1.08	1.05
components				
DDI (w/w %)	53.4	53.3	70.8	71.1
styrene (w/w %)		43.3	26.1	24.8
n-butyl acrylate (w/w %)	43.3			
methacrylic acid (w/w %)	1.3	1.3	0.55	0.77
SDOSS (w/w %)	1.8	1.8	2.3	3.0
$K_2S_2O_8$ (w/w %)	0.26	0.26	0.28	0.40

In view of the above considerations and the results of recent studies,[1] this work focuses on a series of experiments on latexes containing well-defined polystyrene (p-Sty) and poly(*n*-butyl acrylate) (p-nBA) blended particles. While such latex blends can be prepared by mixing two independently polymerized p-Sty and p-nBA polymeric microspheres dispersed in an aqueous medium, latex copolymers containing Sty and nBA moieties in one particle are made by semicontinuous copolymerization. The primary objective of these studies is to assess factors affecting the difference between p-Sty/p-nBA blends and Sty/nBA copolymers during film formation and the effect of latex composition, surfactant mobility, and particle size and temperature effects on the phase separation and dynamics of macromolecular rearrangements during coalescence.

Experimental Section

Latex Synthesis and Film Preparation. Sty, nBA, methacrylic acid (MAA), sodium dioctylsulfosuccinate (SDOSS), and potassium persulfate ($K_2S_2O_8$) were purchased from Aldrich Chemical Co. p-Sty and p-nBA latexes were synthesized by a semicontinuous emulsion polymerization,[21] which was carried out in a 500 mL glass reactor equipped with a reflux condenser, stirrer, and thermometer. The temperature was set at 70 °C, and polymerization reactions were carried out under an inert N_2 atmosphere. The chemical contents of the starting materials for p-nBA and p-Sty latexes with three particle sizes are summarized in Table 1. A pre-emulsion was prepared by mixing deionized H_2O (DDI), SDOSS, nBA, and

10.1021/ma000120r CCC: $19.00
Published on Web 09/07/2000

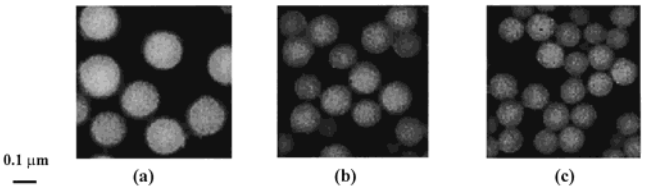

Figure 1. TEM images of p-Sty latexes: (a) 102 nm; (b) 77 nm; (c) 61 nm.

MAA. $K_2S_2O_8$ was dissolved in H_2O (0.87 wt %). The reaction vessel was purged for 20 min with N_2, and at that point, 20 w/w % pre-emulsion was added. When the temperature was raised to 40 °C, one-quarter of the $K_2S_2O_8$ solution was added. When the temperature reached 70 °C, it was held constant until a white, milky emulsion was observed, after which the remaining pre-emulsion and initiator solutions were added slowly. The addition rate of the pre-emulsion and initiator was controlled by a REGLO 100 pump and a universal syringe pump (model 575, Valley Science Co.), respectively. After the pre-emulsion and initiator were added, the system was allowed to react at 75 °C for 3 h to achieve high conversions. p-Sty latexes were synthesized using the same recipe except that the p-Sty latexes with 102, 77, and 61 nm particle sizes were synthesized by varying the amounts of surfactant (Table 1).

Transmission electron microscopy (TEM; JEM-100S, JEOL) was used to determine the particle size and particle size distributions. Particle sizes and their distributions were also measured using a dynamic light-scattering technique (submicron particle size NICOMP 380, PSS−NICOM Particle Sizing Systems). While Table 1 summarizes latex particle sizes synthesized for the purpose of this study, Figure 1 illustrates TEM micrographs of respective p-Sty latexes. An average particle size of p-nBA utilized in this study was 150 nm, whereas p-Sty latex particle sizes were 102, 77, and 61 nm.

Prior to the preparation of latex films with different p-Sty/p-nBA compositions, p-Sty and p-nBA homopolymer suspensions at 25.5% solids were mixed in 50/50, 40/60, 30/70, 20/80, 10/90, and 0/100 w/w % ratios, stirred, and allowed to stand for 10 days before coalescence. Such latex blends were cast on a poly(tetrafluoroethylene) (PTFE) substrate and allowed to coalescence at 80% relative humidity (RH) for 3 days at 25 °C. In a typical experiment, approximately 200 μm thick dry films were prepared.

Spectroscopic Measurements and Quantum Mechanical Computations. Attenuated total reflectance Fourier transform infrared (ATR FT-IR) spectra were collected on a Nicolet Magna-850 FT-IR single-beam spectrometer at a 4 cm^{-1} resolution and a mirror speed of 0.1581 cm s^{-1}. A KRS-5 crystal with a 45° angle and 50 × 20 × 3 mm dimensions was used. Each spectrum represents 200 co-added scans ratioed to 200 reference scans collected using an empty ATR cell. All spectra were corrected for spectral distortions and optical effects using Q-ATR software.[22]

Microscopic ATR FT-IR spectra were collected using a IRμs/Nic-Plan molecular microanalysis system (Nicolet Instruments, Inc.). Latex samples were analyzed using an ATR objective in a reflectance mode equipped with a ZnSe crystal. Surfaces were mapped using the same contact pressure between the ZnSe crystal and latex specimens. Each spectrum was recorded at a 4 cm^{-1} resolution, and 200 scans were co-added using a 3.2 mm circular aperture.

Circle ATR FT-IR spectra of SDOSS, SDOSS + H_2O (1.8 w/w %), and SDOSS + MAA (1.8 w/w%) were collected on a Nicolet Magna-850 FT-IR single-beam spectrometer at a 4 cm^{-1} resolution and a mirror speed of 0.3165 cm s^{-1}. A ZnSe circular crystal with an incidence angle of 45° was used. Each spectrum represents 200 co-added scans ratioed to 200 scans collected on an empty ATR cell. All spectra were corrected for spectral distortions and optical effects using Q-ATR software.[22]

Glass transition temperatures (T_g) of latex films were measured using a dynamic mechanical thermal analysis instrument (Rheometric Scientific DMTA 3E), set at a dynamic temperature ramp of 3 °C/min, an oscillating frequency of 1 Hz, and a strain of 0.5% in the temperature range from −100 to +200 °C.

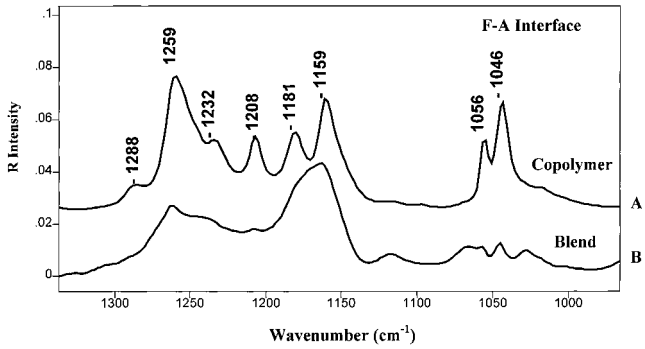

Figure 2. ATR FT-IR spectra in the 1410−970 cm^{-1} region of 50/50 Sty/nBA copolymer and p-Sty/p-nBA blend latex films recorded from the F−A interface: (A) copolymer latex; (B) blended latex (coalescence time = 3 days; RH = 80%).

SDOSS, SDOSS···H_2O, and SDOSS···COOH interactions were calculated using the HyperChem software package (Hypercube, Inc.) that utilizes semiempirical quantum-mechanical AM1 calculations and the geometry optimization program based on the Polak-Ribiere algorithm with a total root-mean-square (rms) gradient of 0.01 kcal/Å·mol.

Surfactant Coverage of Latex Particles. Latex particle surfactant coverages were estimated based on a particle size and the SDOSS difference between the amount of surfactant utilized during synthesis and the amount of free SDOSS solublized in an aqueous phase. Surfactant dissolved in an aqueous phase was determined using the following protocol: (1) Aqueous solutions with various SDOSS concentration levels were prepared in order to obtain a calibration curve and to determine the linear absorption coefficient for the S−O stretching band (0.017 L/mol·cm) at 1046 cm^{-1}. (2) Each latex suspension was centrifuged using a Beckman L8-55M ultracentrifuge at 18 000 rpm set at 20 °C for 4 h, and an aqueous phase was separated from a solid phase for the purpose of SDOSS analysis using a Circle ATR cell.

Results and Discussion

Parts a−c of Figure 1 illustrate TEM micrographs of p-Sty latexes containing 102, 77, and 61 nm particles, respectively. Using these p-Sty particle sizes, latex blends containing p-Sty and 150 nm diameter p-nBA particles will be examined. Traces A and B of Figure 2 represent ATR FT-IR spectra in the 1410−970 cm^{-1} region recorded from the F−A interface of a 50/50 Sty/n-BA copolymer latex and 50/50 p-Sty/p-nBA latex blends with particle sizes of 102 nm (p-Sty) and 150 nm (p-nBA). An employed ATR FT-IR experimental setup allowed us to record the spectra from an approximate average depth of 1.9 μm from the F−A interface.[22] [The average depth thickness was determined using the equation $d_p = \lambda_0/[2\pi\eta_1(\sin^2\theta - \eta_{21})^{1/2}]$, where λ_0 is the wavelength of light, η_1 is the refractive index of the crystal, θ is the angle of incidence, η_{21} is the refractive index ratio of the sample and the crystal. All spectra were corrected using the Urban−Huang algorithm[21] in an effort to eliminate spectral distortions resulting from the refractive index changes.] As seen in Figure 2, trace A, significantly enhanced intensities of the SDOSS bands at 1056 and 1046 cm^{-1} due to S−O symmetric stretching modes of $SO_3^-Na^+$···COOH and $SO_3^-Na^+$···H_2O associations[3−12] are detected at the F−A interface of the copolymer latex. At the same time, only traces of SDOSS are detected in trace B. Although these results explicitly show that, in comparison to the Sty/

nBA copolymer,[1] only small quantities of SDOSS exude to the F−A interface in blended latex films, this behavior is somewhat surprising because one perhaps would anticipate that the presence of hydrophobic polystyrene spheres would enhance the mobility of ionic SDOSS.

In view of the above data and postponing temporarily the analysis of the SDOSS behavior in blended and copolymerized latexes, let us consider the effect of phase separation in blended latexes. For that reason DMTA analysis was performed to measure tan δ values as a function of temperature. In these experiments, the maximum tan δ values correspond to the T_g of 50/50 p-Sty/nBA copolymer and p-Sty/p-nBA blends. The DMTA analysis (not shown) indicated the presence of one T_g at 20 °C for copolymer latexes, thus indicating that no detectable phase separation within the copolymer latex components occurred. However, for a p-Sty/p−nBA latex blend, two T_g's were detected at −35 and +110 °C, which are due to p-nBA and p-Sty phases, respectively.

In the context of the above data, the next question to be addressed is the effect of phase separation on the exudation behavior of SDOSS. For Sty/nBA copolymer with the MFT below the coalescence temperature (T_c), formation of the continuous phase is typically determined by the ability of particle packing, their deformation, and interdiffusion. For 50/50 p-Sty/p-nBA latex blends, lower levels of SDOSS molecules are detected at the F−A interface (Figure 2, trace B), which indicates that the film formation affects the migration of SDOSS. Because the temperature difference between T_c and T_g of the latex polymer has a significant effect on the coalescence, and thus may influence migration of SDOSS, blended latex films were annealed at 50, 75, 90, and 120 °C for 2 h, followed by cooling to 25 °C and recording ATR FT-IR spectra from the F−A and F−S interfaces. Furthermore, in an effort to determine the effect of the latex composition on SDOSS migration, 50/50, 40/60, 30/70, 20/80, 10/90, and 0/100 p-Sty/p-nBA blends were prepared. ATR FT-IR spectra of p-Sty/p-nBA latex blends exposed to annealing temperatures of up to 120 °C with different compositions are shown in Figure 3a−f. For 0/100 (Figure 3a), 10/90 (Figure 3b), and 20/80 (Figure 3c) p-Sty/p-nBA ratios, intensities of the bands at 1046 and 1056 cm^{-1} due to SDOSS surfactant molecules remain the same when annealing is conducted between 25 and 90 °C, and only a slight increase is observed at 120 °C. These results show that, when the p-nBA content is high, which for these compositions is the primary source of SDOSS, SDOSS, and p-nBA, phases appear to be compatible. When latex blends contain higher p-Sty contents, such as in the case of 30/70 (Figure 3d), 40/60 (Figure 3e), and 50/50 (Figure 3f) p-Sty/p-nBA, the bands at 1046 and 1056 cm^{-1} increase when the annealing temperature is set at 90 °C. However, when the annealing temperature is raised to 120 °C, the same bands significantly increase, indicating exudation of SDOSS to the F−A interface. Furthermore, for latex films containing higher concentration levels of p-Sty, when the annealing temperature is above 120 °C, the band 1046 and 1056 cm^{-1} intensities at the F−A interface increase. These results show that the amount of surfactant migration to the F−A interface is affected by the surfactant−polymer compatibility, which also depends on the T_c. No SDOSS stratification was detected when the blended latex is coalesced between 25 and 75 °C, suggesting that surfactant molecules are most likely imbedded in the p-Sty particle surfaces. Upon annealing at 120 °C, which is above the T_g of the p-Sty phase, SDOSS molecules become mobile because of increased p-Sty free volume and migrate to the F−A interface.

On the basis of the above data, one can depict the SDOSS behavior in pure p-nBA and 50/50 p-Sty/p-nBA latex blends, which is schematically shown in Figure 4. When pure p-nBA latexes are coalesced at 25 °C, latex particles deform and interdiffuse and no SDOSS is detected at the F−A interface because of good compatibility between p-nBA/SDOSS (Figure 4a).[1] For 50/50 p-Sty/p-nBA latex blends (Figure 4b) coalesced at 25 °C, only small amounts of SDOSS are detected at the F−A interface, but when latex films are annealed at 120 °C, SDOSS molecules migrate to the F−A interface.

As we recall, for the p-Sty/p−n-BA latex blends, DMTA analysis showed the presence of two T_g's detected at −35 and +110 °C, which are due to p-nBA and p-Sty phases, respectively. Thus, the question one needs to impose is whether there is a correlation between the SDOSS mobility and the phase separation. For that reason, we prepared 50/50 p-Sty/p-nBA latex blends with various p-Sty particle sizes that were defined in Figure 1. Although one would anticipate that, for a given volume, smaller particles exhibit a larger total surface, and therefore higher concentration levels of SDOSS, this issue should be examined. This is quite important in the context of these as well as previous studies[3−13] because one may be concerned, and rightfully so, that the presence of SDOSS near the F−A interface results from its excessive concentration levels in an aqueous phase. In an effort to establish if there are free SDOSS molecules in the latex aqueous phase, latex solutions were centrifuged and an aqueous phase was separated from solid latex particles. Such an aqueous solution was analyzed using Circle ATR FT-IR, and the resulting spectra are shown in Figure 5. Part A of this figure is a calibration curve that illustrates the relationship between the linear absorptivity of the 1046 cm^{-1} band and the SDOSS concentration, which serves to quantitatively determine the amount of SDOSS. As we recall, 1.8 w/w % of SDOSS was utilized in the latex synthesis and trace A of Figure 5b illustrates the spectrum of 1.8 w/w SDOSS solubilized in water. As can be seen, the 1046 and 1208 cm^{-1} bands dominate over other spectral features. However, when an aqueous phase is separated from the latex particles and the aqueous portion is analyzed, traces B−E of Figure 5b result. As can be seen, a series of spectra of the aqueous phases separated from latex particle solutions of p-nBA (particle size of 150 nm; trace B) and p-Sty (particle sizes of 102, 77, and 61 nm; traces C−E) show only very weak bands due to SDOSS. Thus, the source of SDOSS migrating to the F−A interface is not an aqueous phase. Using a calibration curve shown in Figure 5a, the 1046 cm^{-1} band intensities were quantified to determine the actual SDOSS concentration levels in the aqueous phase. It turns out that only 4−9% of the total amount of SDOSS (1.8, 2.3, and 3.0 w/w %) utilized to prepare 61, 77, and 102 nm p-Sty latex particle suspensions is detected in the aqueous phases separated from latex solutions. These amounts cannot certainly account for significantly higher concentration levels of SDOSS near the F−A interface (Figure 3f, trace A). As a matter of fact, one can estimate that, when p-nBA and p-Sty particles are

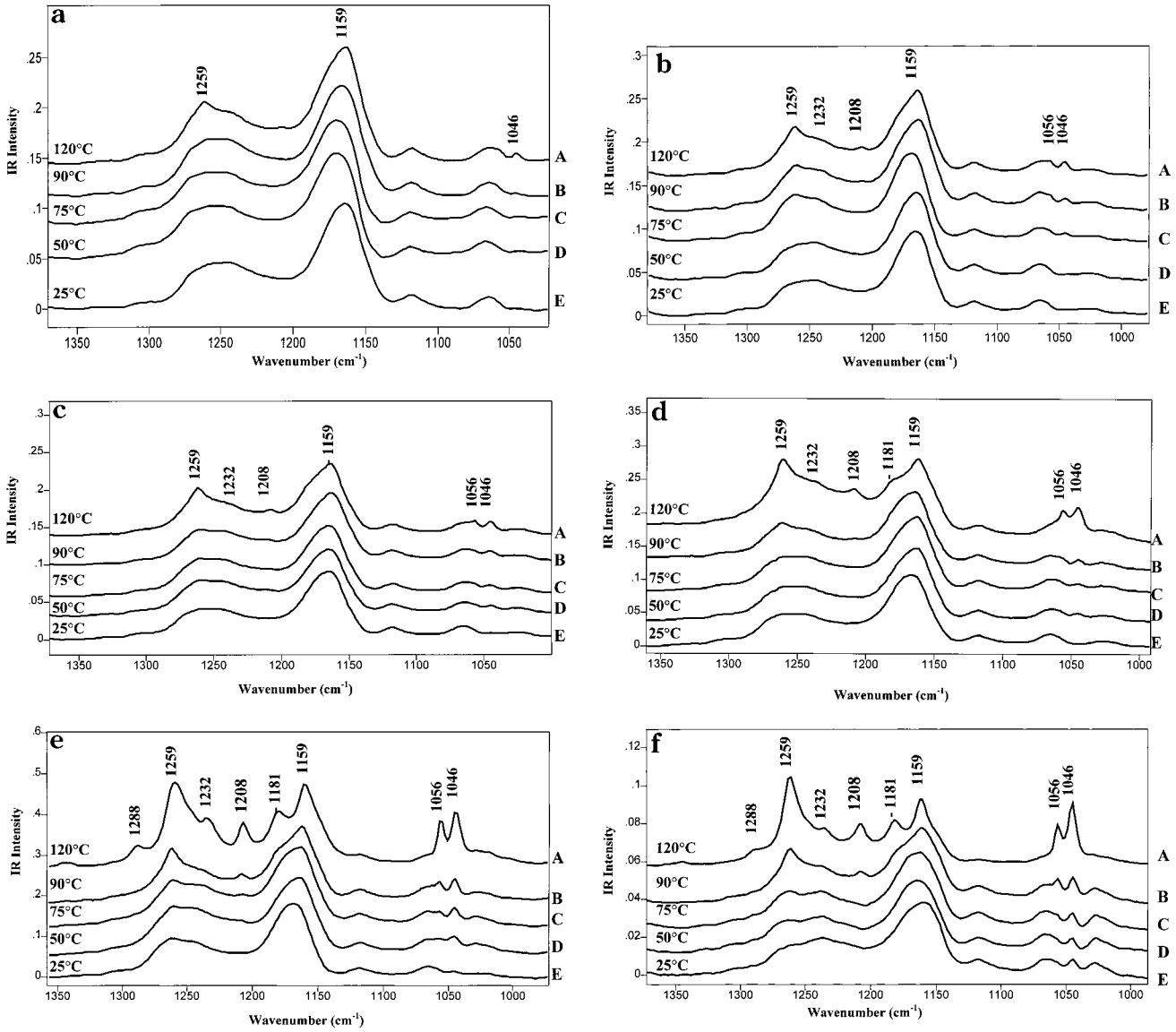

Figure 3. ATR FT-IR spectra in the 1370−970 cm^{-1} region of p-Sty/p-nBA latex blends containing different p-Sty/p-nBA ratios recorded from the F−A interface as a function of the annealing temperature: (a) 0/100 p-Sty/p-nBA; (b) 10/90 p-Sty/p-nBA; (c) 20/80 p-Sty/p-nBA; (d) 30/70 p-Sty/p-nBA; (e) 40/60 p-Sty/p-nBA; (f) 50/50 p-Sty/p-nBA. Traces A−E of parts a−d correspond to 120, 90, 75, 50, and 25 °C annealing temperatures.

monodispersed and using the density values for p-Sty and p-nBA[23] as well as the surface areas of the particles, the estimated SDOSS coverages for p-nBA (150 nm) and p-Sty (102, 77, and 61 nm) particles are 2.31×10^{-10}, 1.60×10^{-10}, 2.41×10^{-10}, and 2.60×10^{-10} mol/cm^2, respectively. These results are listed in Table 2, and it should be noted that the estimated SDOSS particle coverages are not exactly the same for all particle sizes because different initial amounts of SDOSS were used in order to obtain different particle sizes.

With these data in mind and considering the fact that the T_c has a significant effect on the migration of SDOSS molecules, latex films were annealed at 50, 75, 90, and 120 °C for 2 h, followed by cooling them down to 25 °C. Such films were analyzed using ATR FT-IR to quantitatively determine[21] the surface content changes at the F−A interface as a function of annealed temperatures. As previously reported model studies[13] showed, the first step in this analysis is to determine an absorption coefficient of the bands of interest, which for the 1046 cm^{-1} band due to SDOSS−H_2O interactions is 0.017 L/mol·cm whereas for the 1056 cm^{-1} band resulting from the SDOSS−COOH entities is 0.14 L/mol·cm.[13] Using a double KKT approach,[22] it is then possible to determine the SDOSS volume concentration changes as a function of temperature. These results are shown in Figure 6a,b for p-Sty particle sizes of 61, 77, and 102 nm (curves A−C, respectively). As shown in Figure 6a, curves A−C, as the annealing temperature increases from 25 to 90 °C, SDOSS−H_2O concentration levels slightly increase. However, at 120 °C, the band due to SDOSS−H_2O significantly increases, and it appears that, for 61, 77, and 102 nm p-Sty particle blends, the volume concentration levels at approximately 1.9 μm from the F−A interface are 2.96×10^{-3}, 2.28×10^{-3}, and 1.71×10^{-3} mmol/cm^3, respectively. Similar results are obtained for the SDOSS···COOH interactions (Figure 6b); when films are annealed at 120 °C, the concentration levels for 61, 77, and 102 nm p-Sty latex blends are 2.40×10^{-4}, 2.21×10^{-4}, and 1.87×10^{-4} mmol/cm^3, respectively. Table 2 summarizes the total volume concentrations for COOH−SDOOS and H_2O··· SDOSS interactions and also provides their normalized values. It is apparent that their normalized volumes

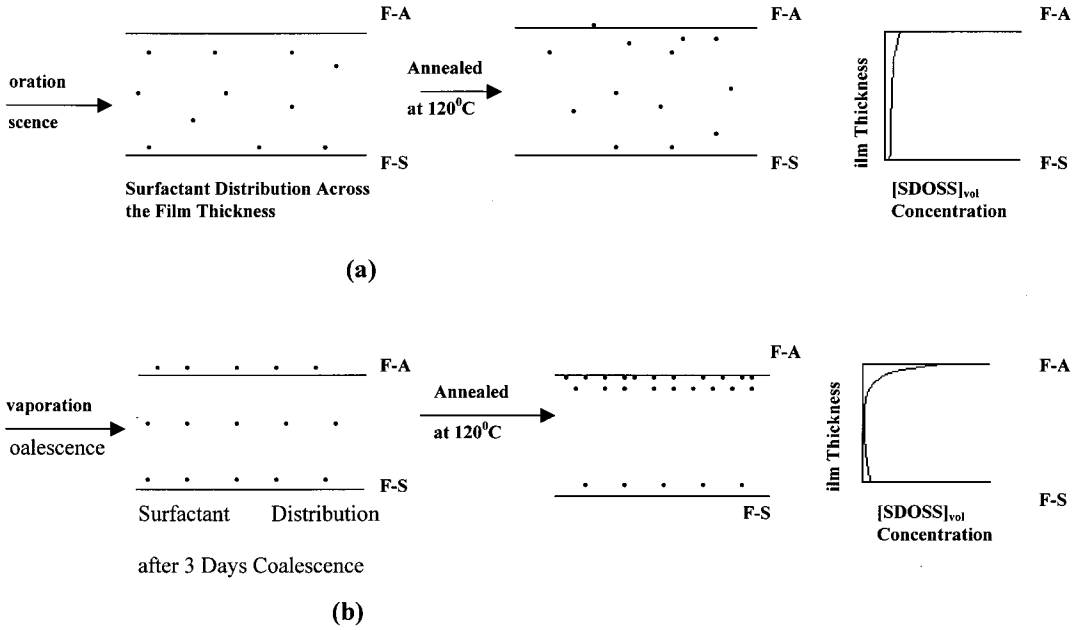

Figure 4. Schematic diagrams illustrating the surfactant behavior for the following latex mixtures: (a) 100% p-nBA latex; (b) 50/50 p-Sty/p-nBA latex blend.

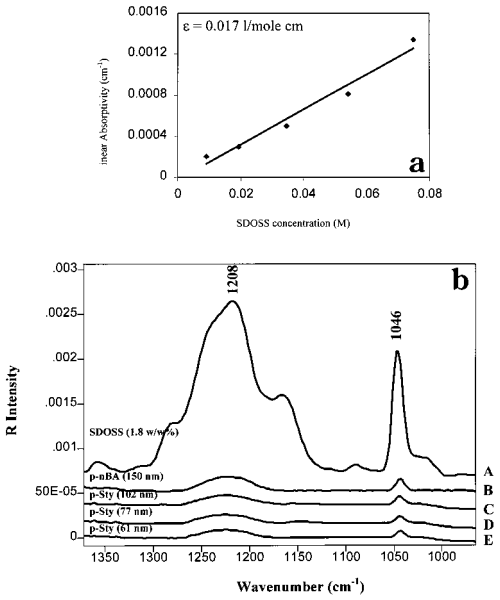

Figure 5. (a) Linear absorption of the 1046 cm^{-1} band plotted as a function of the SDOSS concentration. (b) Trace A, 1.8 w/w % SDOSS in water; trace B, a Circle ATR FT-IR spectrum of an aqueous phase centrifuged from a 150 nm p-nBA emulsion; trace C, a Circle ATR FT-IR spectrum of an aqueous phase centrifuged from a 102 nm p-Sty emulsion; trace D, a Circle ATR FT-IR spectrum of an aqueous phase centrifuged from a 77 p-nBA emulsion; trace E, a Circle ATR FT-IR spectrum of an aqueous phase centrifuged from a 61 nm p-nBA emulsion.

near the F−A interface obtained from ATR FT-IR measurements parallel the normalized p-Sty particle surface area ratios. Thus, the primary source of exudation of SDOSS in p-Sty/p-nBA latex blends is the p-Sty phase, and when specimens are annealed above the T_g of p-Sty, phase exudation is detected. As illustrated in Figure 6a,b, higher concentration levels of SDOSS for smaller p-Sty particles provide a source for expelling larger amounts of SDOSS.

Based on these data, the effect of the particle size on the distribution of SDOSS during p-Sty/p-nBA latex blend coalescence can be proposed. This is schematically illustrated in Figure 7, and for the 50/50 p-Sty/nBA latex blend, the latex film formation is depicted by the following stages: (A) liquid dispersion, due to water evaporation, forms a denser film (B), and the particles come into contact with each other. At 25 °C, p-nBA particles deform to flow around the p-Sty particles (C), and after the film is formed, only small quantities of SDOSS are detected at the F−A interface for three p-Sty particle sizes. However, when the same films are annealed at 120 °C (D), SDOSS molecules migrate to the F−A interface, and a significantly higher content of SDOSS is detected for smaller p-Sty particle sizes. This is illustrated in part E of Figure 7, which shows concentration profiles of SDOSS as a function of film thickness for 102, 77, and 61 nm p-Sty particle sizes. As can be seen, at approximately 1.9 μm from the surface, the particle size, and therefore the surface area, plays a significant role in the mobility of SDOSS. At greater depths from the F−A interface, the SDOSS distribution varies, but no detectable particle size effect is observed. These conclusions are based on the step-scan photoacoustic FT-IR results (not shown),[20,24] which indicated that at about 13 μm there is no surfactant present and its concentration is higher again closer to the F−S interface.

Although there are reports[25,26] concerned with the orientation of the most outer molecular entities on surfaces, orientation of SDOSS molecules, especially their hydrophilic ends near the F−A interface, is of interest because the molecules may affect numerous properties including wettability, adhesion, and others. When 50/50 p-Sty/p-nBA blend films are annealed at 120 °C, ATR FT-IR spectra recorded using 90° (TE = transverse electric) and 0° (TM = transverse magnetic) polarizations exhibit spectral features shown in Figure 8. It is quite apparent that the bands at 1046 and 1056 cm^{-1} exhibit significantly higher intensities when ATR FT-IR spectra are recorded using TE polarization. As we recall, polarization experiments allow estimation of the preferential orientation of surface groups,[28] in which the term TE refers to parallel orientation of the electric

Table 2. Estimated SDOSS Coverage of p-Sty Latex Particles

	model latexes			
	p-nBA	p-Sty	p-Sty	p-Sty
latex particle size (nm)	150	102	77	61
density[a] (g/cm^3)	1.087	1.05	1.05	1.05
theoretical latex particle coverage with SDOSS (mol/cm^2)	2.31×10^{-10}	1.60×10^{-10}	2.41×10^{-10}	2.60×10^{-10}
particle surface area ratio[b]		1	1.32	1.66
vol concn (mmol/cm^3) for COOH−SDOSS and H_2O−SDOSS interactions from ATR FT-IR measurements		1.90×10^{-3}	2.50×10^{-3}	3.20×10^{-3}
normalized vol concn for COOH−SDOSS and H_2O−SDOSS interactions from ATR FT-IR measurements		1	1.318	1.687

[a] From ref 23. [b] The particle surface area was normalized to a 102 nm particle size.

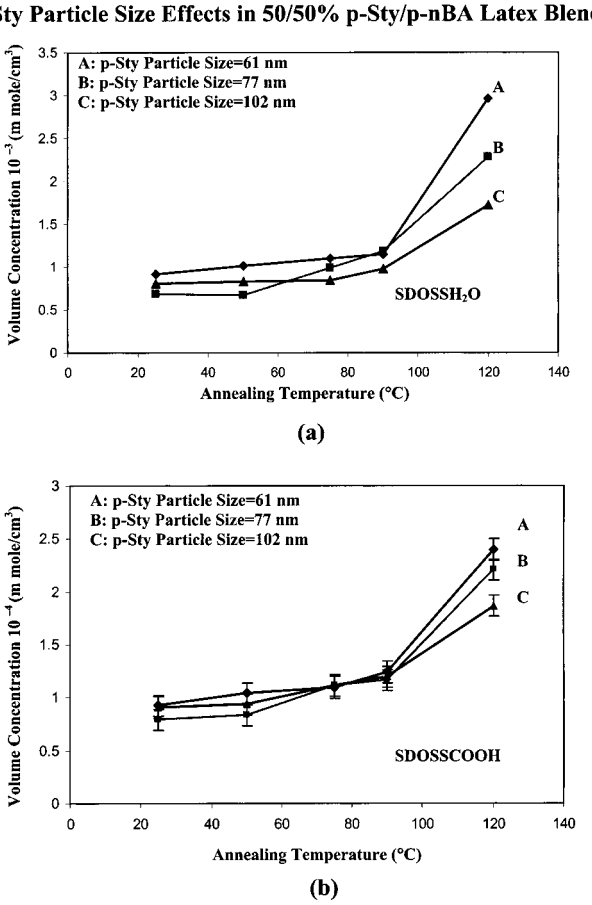

Figure 6. Volume concentration changes of (a) SDOSS···H_2O and (b) SDOSS···COOH interactions plotted as a function of the annealing temperature for 61 (curve A), 77 (curve B), and 102 nm (curve C) p-Sty particle sizes.

vector of electromagnetic radiation whereas TM refers to perpendicular orientation.[27] Further analysis of ATR FT-IR spectra of 50/50 p-Sty/p-nBA blend films recorded using TE (trace A) and TM (trace B) polarizations shows that the band intensities at 1259 and 1208 cm^{-1} due to asymmetric S−O stretching modes resulting from $SO_3^-Na^+$−COOH and $SO_3^-Na^+$−H_2O interactions and those at 1056 and 1046 cm^{-1} due to S−O symmetric stretching modes of $SO_3^-Na^+$−COOH and $SO_3^-Na^+$−H_2O entities exhibit higher intensities (trace A). In contrast, the bands at 1288 and 1232 cm^{-1} due to asymmetric stretching modes of the C−O−C entities resulting from H bonding between COOH and H_2O with SDOSS, and the 1407 cm^{-1} due to CH_2 deformation modes of SDOSS, are significantly stronger when the spectra are recorded using TM polarization (trace B). These results indicate that the orientation of SO_3Na^-−COOH and $SO_3^-Na^+$−H_2O interactions is preferentially parallel to the F−A interface, whereas the C−O−C groups and hydrophobic long CH_2 chains of SDOSS are preferentially perpendicular.

Although this spectroscopic information contains information about orientation, determination of the actual orientation of the SDOSS different entities requires further analysis. In an effort to establish the relationship between the SDOSS structure and its orientation with respect to the film surface, calibration experiments and semimechanical quantum-mechanical calculations were employed. Traces A−C of Figure 9 illustrate Circle ATR FT-IR spectra of SDOSS, SDOSS + H_2O, and SDOSS + MAA mixtures, respectively, in the $SO_3^-Na^+$ region. The band at 1050 cm^{-1} detected in SDOSS (trace A) is attributed to the S−O symmetric stretching modes of $SO_3^-Na^+$ groups, whereas the bands at 1046 and 1056 cm^{-1} are attributed to the S−O symmetric stretching modes of $SO_3^-Na^+$···H_2O (trace B) and $SO_3^-Na^+$···COOH (trace C), respectively. Although in the earlier studies we already establish the origin of these bands, it is appropriate to identify how the local environment and geometry of the sulfonate groups will be affected by these interactions.[15] There are four possible local symmetries of the $SO_3^-Na^+$ group that need consideration: tetrahedral arrangement (T_d), tetragonal plane (D_{4h}), tetragonal pyramidal (C_{4v}), and an irregular tetrahedral arrangement (C_{3v}). For the central sulfur atom surrounded by heterogeneous atoms (three oxygens and carbon), only the tetragonal pyramidal structure with dp^3 and d^3p orbital configurations or the irregular tetrahedral arrangement with dp^3, d^3p, and d^2sp orbital configurations are possible.[28]

Although one would expect that hydrogen bonding may play some role because of the presence of weak acid groups which may disturb the $SO_3^-Na^+$ environment by formation of a partial π double bond between sulfur and oxygen,[14] considering the group theory predictions, let us determine to what extent the $SO_3^-Na^+$ local symmetry is affected by the presence of H_2O and COOH groups. For that reason, we utilized quantum-mechanical calculations, followed by geometry optimization based on the Polak−Ribiere algorithm method. The minimized energy structures and theoretically predicted IR bands for SDOSS, SDOSS−H_2O, SDOSS−HOOC−CH_3, and SDOSS associated with both H_2O and CH_3−COOH entities are shown in Figure 10a−d, respectively. As can be seen in Figure 10a, the calculated symmetric S−O stretching band in SDOSS is 1058 cm^{-1}. As anticipated, this band shifts to the lower S−O stretching energy when SDOSS−H_2O interactions are present. Indeed, the calculated S−O stretching band is found at 1054 cm^{-1}. SDOSS−COOH associations are represented by the 1071 cm^{-1} band (Figure 10c). These structures

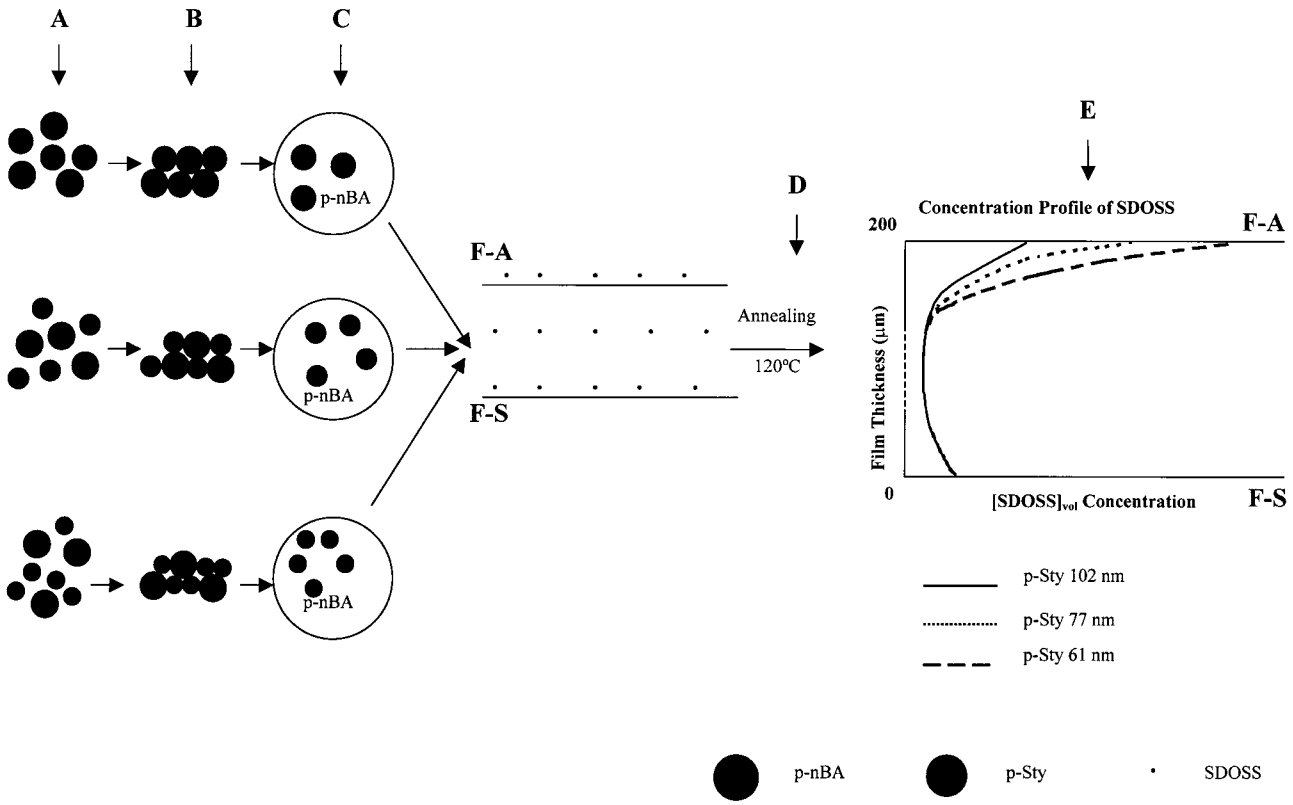

Figure 7. Schematic diagram of the effect of the particle size on the distribution of SDOSS in latex films during p-Sty/p-nBA latex blend coalescence.

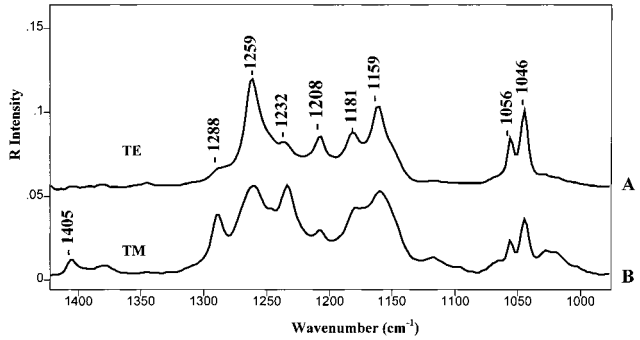

Figure 8. ATR FT-IR spectra in the 1430−970 cm^{-1} region of a 50/50 p-Sty/p-nBA latex blend recorded from the F−A interface after annealing at 120 °C: (A) 90° polarization (TE); (B) 0° polarization (TM).

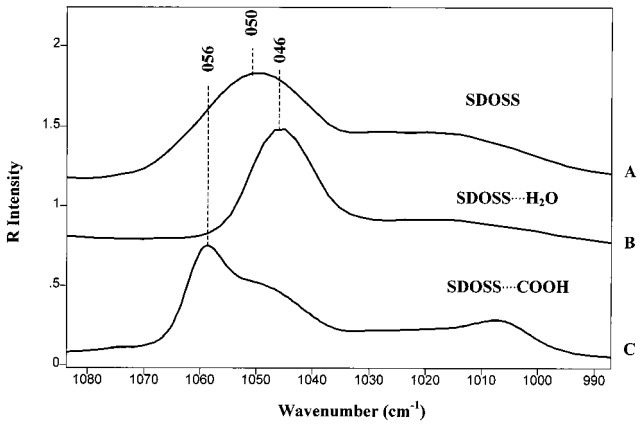

Figure 9. (A) Transmission FT-IR spectrum of solid SDOSS. (B) Circle ATR FT-IR spectrum of SDOSS solubilized in water (1.8 w/w %). (C) Circle ATR FT-IR spectrum of SDOSS (1.8 w/w %) solubilized in methacrylic acid.

are further confirmed in Figure 10d, where quantum-mechanical calculations in the presence of H_2O and COOH result again in the 1054 and 1071 cm^{-1} bands. Thus, these results are in agreement with the Circle ATR FT-IR experiments (Figure 9), and although there is no exact vibrational energy match because of the fact that this methodology is limited by the inability of predicting more than two interactions at a time, considering a 4 cm^{-1} experimental resolution, the trends are the same. Another conclusion from the quantum-mechanical calculations is that, for SDOSS, SDOSS−H_2O, and SDOSS−HOOC−CH_3 entities, the $-SO_3^-Na^+$ local symmetry remains unchanged and the O−S−O and O−S−C angles at 113−114° and 102−105° (Figure 10a−d), respectively, are maintained regardless of H_2O and COOH interactions. These results indicate that the $SO_3^-Na^+$ geometry and the bond length are not affected by the presence of H_2O and COOH groups. Thus, the parameter that is affected by these interactions is the force constant of the S−O bond. It should be also noted that even the formation of partial π double bonds does not affect the local $SO_3^-Na^+$ geometry.

In summary, a combination of ATR FT-IR analysis and quantum-mechanical modeling allows us to determine the orientation of SDOSS near the F−A interface of the latex blend films. This is shown in Figure 11, where the orientation of the surfactant molecules near interfacial F−A and F−S regions results from the ability of SDOSS to compensate of the access of surface free energy in order to compensate for the interfacial surface tension.[29] Because latex film formation is initiated by water removal, one would anticipate that, at this stage, if any SDOSS molecules were present in an aqueous

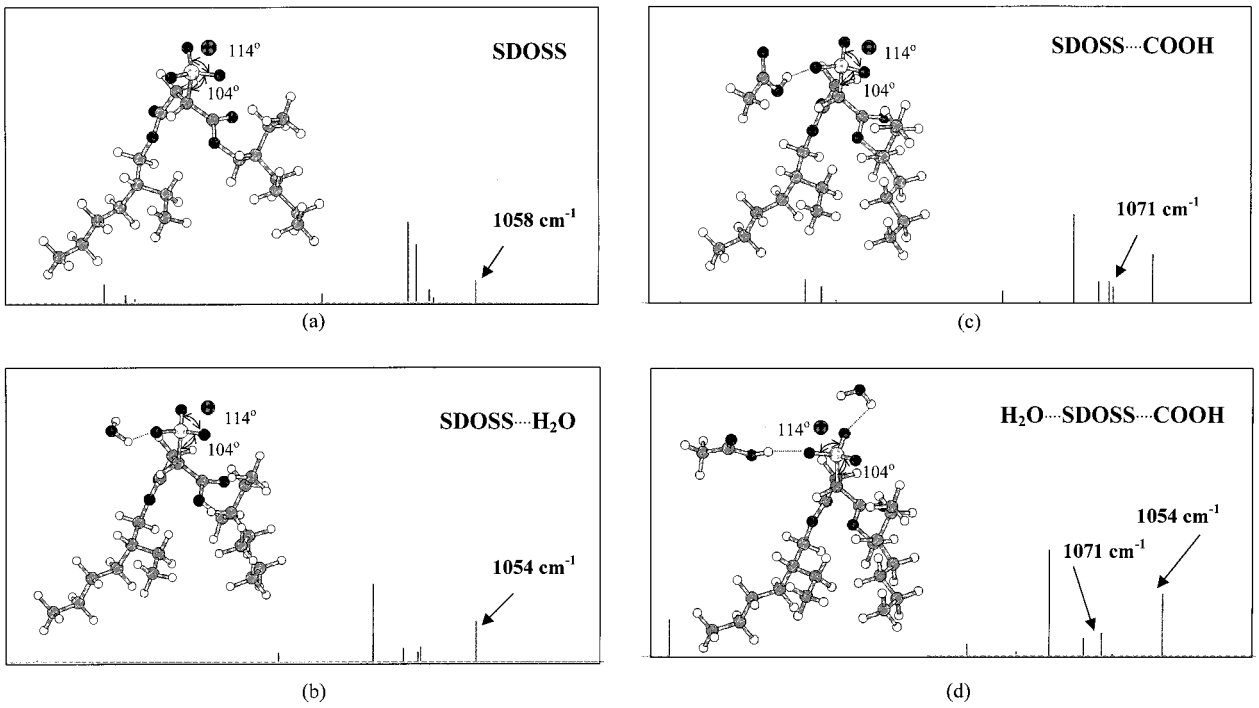

Figure 10. $Na^+SO_3^-$ local geometry predictions and theoretically determined IR bands for (a) SDOSS, (b) SDOSS···H_2O associations, (c) SDOSS···HOOC−CH_3 associations, and (d) SDOSS simultaneous associations with H_2O and CH_3−COOH.

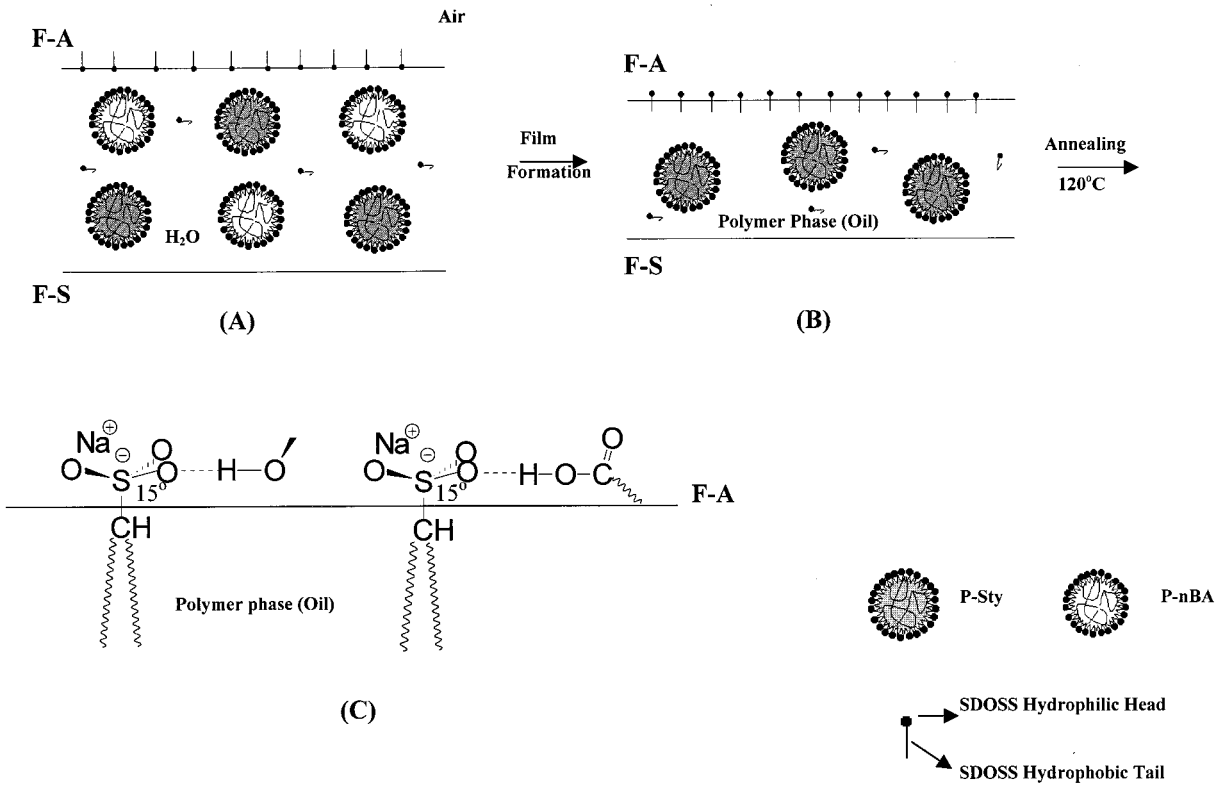

Figure 11. Self-assembled surface of latex films containing SDOSS end groups associated with COOH and H_2O: The SO_3Na^+··· COOH and $SO_3^-Na^+$···H_2O interactions are preferentially parallel to the F−A interface. The C−O−C groups and long hydrophobic CH_2 chains of SDOSS are preferentially perpendicular to the F−A latex interface. It should be realized that ATR FT-IR measurements provide no evidence for the formation of monolayers, although their formation is possible.

phase and we detected 4−9% of the initial SDOSS concentration, they would align perpendicularly to the liquid−vapor surface, with hydrophobic groups being perpendicular and away from the liquid−vapor interface. This is schematically illustrated in Figure 11A. As water is removed, similar SDOSS concentration levels are detected, but their orientation changes because of hydrophobic interactions with the latex polymer (Figure 11B). Further annealing at 120 °C results in the diffusion of SDOSS to the F−A interface. When SDOSS molecules migrate to the F−A interface, as a result of the increasing free volume in the p-Sty phase, thus

allowing the SDOSS release, hydrophobic tails take preferentially a perpendicular orientation to the surface promoted by hydrophobic interactions between alkyl chains of SDOSS and the latex surface. On the other hand, hydrophilic groups stay away from the oil phase because of the reduction of the contact area of hydrophilic $SO_3^-Na^+$/hydrophobic polymers (p-Sty and p-nBA). This is schematically shown in Figure 11C. In fact, hydrophobic chains of SDOSS associated with latex polymers are preferentially perpendicular to the surface, which is demonstrated by a significantly stronger C−O−C symmetric stretching band at 1288 cm^{-1} recorded using TM polarization (Figure 8). In contrast, $SO_3^-Na^+$ groups associated with H_2O and −COOH entities tend to be away from the latex polymer and are preferentially parallel to the film surface. Semiempirical quantum-mechanical calculations also show that, in order for these species to sustain a minimum energy state, the preferred angle between S−O bonds and the film surface is about 15°, which is consistent with the ATR FT-IR trends shown in Figure 8, indicating a preferential parallel orientation of hydrophilic $SO_3^-Na^+$ groups to the latex surface. It should be pointed out that, although a pictorial representation of SDOSS shown in Figure 11 may suggest a monolayer assembly of SDOSS on the latex surface, at this point there is no evidence that this is the case, because ATR FT-IR measurements conducted in these studies represent SDOSS volume measurements given by the penetration depth.

Conclusions

When p-Sty/p-nBA latex films are coalesced at 25 °C, only a small fraction of SDOSS is detected at the F−A interface. However, when the coalescence temperature is above the p-Sty phase, exudation of SDOSS molecules to the F−A interface is excessive. The composition of latex blends also has a significant effect on the SDOSS mobility. At 120 °C, lower concentration levels of SDOSS are detected at the F−A interface for latex blends with a higher p-nBA content. Quantitative ATR FT-IR analysis of the F−A interface of 50/50 p-Sty/p-nBA latex blends shows that, at 120 °C, SDOSS···H_2O volume concentrations are 2.96×10^{-3}, 2.28×10^{-3}, and 1.71×10^{-3} mmol/cm^3 for 61, 77, and 102 nm p-Sty latexes, respectively. Concentration levels of SDOSS···COOH associations are 2.40×10^{-4}, 2.21×10^{-4}, and 1.87×10^{-4} mmol/cm^3 for 61, 77, and 102 nm p-Sty latexes, respectively. These studies also show that the amount of SDOSS exuding the F−A interface is proportional to the surface area of p-Sty particles. ATR FT-IR polarization studies show that hydrophilic ends of SDOSS associated with H_2O and COOH are preferentially parallel to the film surface and hydrophobic chains of SDOSS are preferentially perpendicular to the surface but that the local geometry of the $SO_3^-Na^+$ groups is not affected by the presence of H_2O and COOH groups.

Acknowledgment. The authors are thankful to the National Science Foundation Industry/University Cooperative Research Center in Coatings for financial support of these studies.

References and Notes

(1) Zhao, Y.; Urban, M. W. *Macromolecules* **2000**, *33*, 2184.
(2) Ramarai, B.; Rajalingam, P.; Radhakrishnan, G. *J. Appl. Polym. Sci.* **1991**, *43*, 23.
(3) Niu, B.-J.; Urban, M. W. *J. Appl. Polym. Sci.* **1995**, *56*, 377.
(4) Niu, B.-J.; Urban, M. W. *J. Appl. Polym. Sci.* **1996**, *60*, 371.
(5) Urban, M. W.; Evanson, K. W. *Polym. Commun.* **1990**, *31*, 279.
(6) Thorstenson, T. A.; Evanson, K. W.; Urban, M. W. *Polym. Mater. Sci. Eng.* **1991**, *64*, 195.
(7) Thorstenson, T. A.; Tebelius, L. K.; Urban, M. W. *J. Appl. Polym. Sci.* **1993**, *49*, 103.
(8) Evanson, K. W.; Thorstenson, T. A.; Urban, M. W. *J. Appl. Polym. Sci.* **1991**, *42*, 2309.
(9) Thorstenson, T. A.; Evanson, K. W.; Urban, M. W. *Structure−Property Relations in Polymers: Spectroscopy and Performance*; Urban, M. W., Craver, C. D., Eds.; Advances in Chemistry Series 236; American Chemical Society: Washington, DC, 1993.
(10) Evanson, K. W.; Urban, M. W. *Surface Phenomena and Fine Particles in Water-based Coating and Printing Technology*; Sharma, M. K., Micale, F. J., Eds.; Plenum: New York, 1991; p 197.
(11) Thorstenson, T. A.; Urban, M. W. *J. Appl. Polym. Sci.* **1993**, *47*, 1387.
(12) Thorstenson, T. A.; Urban, M. W. *J. Appl. Polym. Sci.* **1993**, *50*, 1207.
(13) Niu, B.-J.; Urban, M. W. *J. Appl. Polym. Sci.* **1996**, *60*, 389.
(14) Evanson, K. W.; Thorstenson, T. A.; Urban, M. W. *J. Appl. Polym. Sci.* **1991**, *42*, 2297.
(15) Evanson, K. W.; Urban, M. W. *J. Appl. Polym. Sci.* **1991**, *42*, 2287.
(16) Kunkel, J. P. W.; Urban, M. W. *J. Appl. Polym. Sci.* **1993**, *50*, 1217.
(17) Tebelius, L. K.; Urban, M. W. *J. Appl. Polym. Sci.* **1995**, *56*, 387.
(18) Zhao, C. L.; Holl, Y.; Pith, T.; Lambla, M. *Colloid Polym. Sci.* **1987**, *265*, 823.
(19) Thorstenson, T. A.; Urban, M. W. *J. Appl. Polym. Sci.* **1993**, *47*, 1381.
(20) Niu, B.-J.; Urban, M. W. *J. Appl. Polym. Sci.* **1996**, *60*, 379.
(21) Lovell, P. A.; Mohameds, E. A. *Emulsion Polymerization and Emulsion Polymers*; John Wiley & Sons: New York, 1997.
(22) Urban, M. W. *Attenuated Total Reflectance Spectroscopy of Polymers−Theory and Practice*; American Chemical Society: Washington, DC, 1996.
(23) Grulke, E. A. *Polymer Handbook*, 3rd ed.; Wiley-Interscience: New York, 1989.
(24) Urban, M. W. *Macromol. Symp.* **1999**, *141*, 15−31.
(25) Katayama, N.; Ozaki, Y.; Seki, T. *Langmuir* **1994**, *10*, 6.
(26) Suzuki, S.; Isoda, S.; Maeda, M. *Langmuir* **1989**, *5*, 1673.
(27) Zhao, Y.; Urban, M. W. *Langmuir* **1999**, *15*, 3538.
(28) Cotton, F. A. *Chemical Applications of Group Theory*, 2nd ed.; Wiley-Interscience: New York, 1971.
(29) Adamson, G. *Physical Chemistry of Surfaces*, 6th ed.; Wiley-Interscience: New York, 1997.

MA000120R